Mixed spacer cation stabilization of blue-emitting n=2 Ruddlesden-Popper organic-inorganic halide perovskite films

Tik Lun Leung, Ho Won Tam, Fangzhou Liu, Jingyang Lin, Alan Man Ching Ng, Wai Kin Chan, Wei Chen, Zhubing He, Ivor Lončarić, Luca Grisanti, Chao Ma, Kam Sing Wong, Ying Suet Lau, Furong Zhu, Željko Skoko, Jasminka Popović, and Aleksandra B. Djurišić**

T. L. Leung, H. W. Tam, Dr. F. Z. Liu, J. Y. Lin, Prof. A. B. Djurišić
Department of Physics, The University of Hong Kong, Pokfulam Road, Hong Kong
E-mail: dalek@hku.hk

Dr. A. M. C. Ng
Department of Physics, Southern University of Science and Technology, No. 1088, Xueyuan Road, Shenzhen, Guangdong, China

Prof. W. K. Chan
Department of Chemistry, The University of Hong Kong, Pokfulam Road, Hong Kong

W. Chen, Dr. Z. B. He
Department of Materials Science and Engineering, Shenzhen Key Laboratory of Full Spectral Solar Electricity Generation (FSSEG), Southern University of Science and Technology, No. 1088, Xueyuan Road, Shenzhen, China

Dr. I. Lončarić, Dr. L. Grisanti
Division of Theoretical Physics, Condensed Matter and Statistical Physics Group, Ruđer Bošković Institute, Bijenička 54, Zagreb, Croatia

C. Ma, Prof. K. S. Wong
Department of Physics, The Hong Kong University of Science and Technology, Clearwater Bay, Hong Kong

Y. S. Lau, Prof. F. R. Zhu
Department of Physics, Research Centre of Excellence for Organic Electronics and Institute of Advanced Materials, Hong Kong Baptist University, Kowloon Town, Hong Kong

Prof. Ž. Skoko
Department of Physics, Faculty of Science, University of Zagreb, Bijenička 32, Zagreb, Croatia

Dr. J. Popović
Division of Materials Physics, Laboratory for Synthesis and Crystallography of Functional Materials, Ruđer Bošković Institute, Bijenička 54, Zagreb, Croatia
E-mail: jpopovic@irb.hr

Keywords: Ruddlesden-Popper, quasi-2D perovskites, perovskite light-emitting diodes, blue emission

Abstract

Ruddlesden-Popper halide perovskite (RPP) materials are of significant interest for light emitting devices since their emission wavelength can be controlled by tuning the number of layers *n*, resulting in improved spectral stability compared to mixed halide devices. However, RPP films typically contain phases with different *n* and the low *n* phases tend to be unstable upon exposure to humidity, irradiation, and/or elevated temperature which hinders the achievement of pure blue emission from *n*=2 films. In this work, two spacer cations are used to form a RPP film with mixed cation bilayer and high *n*=2 phase purity, improved stability and brighter light emission compared to single spacer cation RPP. The stabilization of *n*=2 phase is attributed to favorable formation energy, reduced strain and reduced electron-phonon coupling compared to the RPP films with only one type of spacer cation. Using this approach, pure blue LEDs with CIE coordinates of (0.156, 0.088) and excellent spectral stability are achieved.

Halide perovskite LEDs, including those based on Ruddlesden-Popper perovskites (RPP), have been attracting increasing attention.[1-4] RPP have a general formula $R_2A_{n-1}B_nX_{3n+1}$, where R^+ is the bulky amine spacer cation, A^+ is an organic cation, B^{2+} is a metal cation, X^- is a halide anion and *n* is the number of perovskite layers between the spacer cations. RP perovskites have been extensively studied[5-32] since the choices of R and *n* enable wider tunability of properties compared to 3D perovskites ABX_3. Emission tuning by changing *n* instead of using halide mixtures enables improved color stability compared to mixed halide LEDs which commonly exhibit peak shifts with time and/or bias due to phase segregation.[3,4,28] However, while exfoliated RPP single crystals exhibit clear dependence of properties on the number of layers *n*, thin films typically consist of a mixture of phases with different *n*[1,10,17,21,23,25,26] and the phase pure films (achieved for one spacer cation via melt-processing instead of commonly used spin-coating) have been scarce.[31] The existence of multiple *n* phases is undesirable for LED applications since it can lead to emission peak shift with increasing bias.[23] Thus, considerable efforts have been made to control the phase composition and layer orientation in RPP thin films, especially those containing common spacer cations such as butylammonium (BA)[6-8,10,24,29,30] and phenethylammonium (PEA).[14,19,20,23,30] Despite these efforts, the differences in behavior (processability, stability and emission efficiency) of the RPP with BA and PEA spacer cations are not well understood, and the blue emitting RPP typically contain multiple peaks in either absorption or emission spectra,[21,23,25,26,28] indicating that phase purity has not been achieved. Furthermore, energy funneling phenomenon,[1,17,20] which involves energy transfer from lower *n* (higher energy) to higher *n* (lower energy) domains resulting in a brighter, but red shifted emission, represents further difficulty in obtaining pure blue emission from *n*=2 RPP emitters. Therefore, green emission[21] or at best sky blue (~490 nm) emission,[23] is usually obtained in LEDs even for predominant *n*=2 composition of the film[21] and suppressed formation of *n*=1 phase using processing additives.

[23] Consequently, there have been only a few reports on RPP LEDs with deep blue to pure blue emission (center emission at ~450-465 nm), and the reported efficiencies have been low (~10^{-3}% for devices emitting <460 nm,[4,21] and 0.15% recently achieved for ~465 nm, <*n*>=3, [28]). Experimental efforts to obtain pure phase *n*=2 films with pure blue emission are further hampered by inadequate theoretical understanding of the RPP formation and the effects of the spacer cation on the material properties, in particular those which can affect the emission efficiency, such as electron-phonon coupling[13] and strain relaxation[33] which affects trap density. Formation energies, bandgaps, etc. reported until today have been calculated by density functional theory (DFT) at 0 K.[5,13,23] Furthermore, electron-phonon coupling in RPP has so far been (only) indirectly addressed, either by means of structural arguments,[34] or based on average displacements through molecular dynamics.[13] Performing DFT calculations at room temperature enables improved understanding of the effect of spacer cation on RPP properties that can be compared to real experimental conditions and offers an insight into the feasibilty of stabilization of *n*=2 perovskite phase by the alternative mixed-cation approach.

In this work, high phase purity *n*=2 films with improved light emission in deep-blue region and improved ambient and thermal stability are achieved in a RPP material which incorporates two different spacer cations (BA and PEA) forming a mixed bilayer, which embodies the processing advantages of BA, as well as high brightness and improved ambient stability of PEA. While the addition of a second spacer cation in solar cells based on higher *n* perovskites can lead to reduced recombination losses,[35-37] improved morphology and crystal orientation,[37] improved ambient stability[35] and reduced phase segregation under laser irradiation,[36] the underlying mechanism has not been understood. To elucidate reasons responsible for the observed phenomena, we performed comprehensive theoretical computations, taking advantage of DFT *ab-initio* molecular dynamics, including van der Waals forces, to improve the evaluation of formation enthalpies and quantify electron-phonon (e-ph) couplings. Formation enthalpies are obtained from NVT ensemble molecular dynamics

at 300 K of each product and reactant, and therefore, in contrast to common static T=0 K approaches, room temperature contributions are also included. Estimation of e-ph couplings is obtained from Fourier transform of time dependent band gaps in NVE ensemble molecular dynamics (see Methods for more details). Theoretical simulations are combined with comprehensive experimental characterisations of the RPP films with pure BA, PEA and mixed BA,PEA spacer cations, and LEDs based on phase pure n=2 films are demonstrated. In terms of efficiency both $(BA_{0.5}PEA_{0.5})_2MAPb_2Br_7$ and $BA_2MAPb_2Br_7$ devices exhibit comparable values of the order of 10^{-2}% which is an order of magnitude higher compared to a previous report with multiple emission peaks for $BA_2MA_{n-1}Pb_nBr_{3n+1}$.[21] However, due to the thermal instability of n=2 phase, EL of pure BA based devices is shifted to 468 nm, resulting in a sky-blue emission with CIE coordinates of (0.132, 0.104). In the case of $(BA_{0.5}PEA_{0.5})_2MAPb_2Br_7$ devices, the improved stability of n=2 phase results in emission centered at 456 nm with CIE coordinates (0.156, 0.088) which are very close to the NTSC pure blue standard (0.14, 0.08).

The results of DFT calculations are summarised in **Figure 1**, **Tables S1, S2, S3** and **Figure S1**, Supporting Information. The calculations show that the formation enthalpies of both $BA_2MAPb_2Br_7$ and mixed cation $(BA_{0.5}PEA_{0.5})_2MAPb_2Br_7$ exhibit the same trend (**Figure 1a)**; in both cases n=2 phase is characterized with the lowest formation enthalpy, compared to n=1 and n=3, indicating that the crystallization of n=2 phase should be possible without the formation of any lower or/and higher n impurities. From an experimental point of view, an appearance of higher n would have been especially bothersome since it often leads to the redshift in emission due to energy funneling. Nevertheless, the calculations showed that the formation enthalpy of n=3 mixed phase is much higher compared to n=2. While this does not preclude the formation of n=1 and n=3 phases under some experimental conditions (especially taking into account the formation of solvent intermediates, solubility differences and their effect on crystallization), it is a clear indication that there exist conditions under which it is

possible to obtain phase-pure films. On the other hand, our theoretical estimation suggests that a mixture of phases should be expected in the case of PEA-based perovskite. **Figure 1a** shows that n=1 phase has the lowest formation enthalpy but we can notice that the formation enthalpies for different values of n are also quite similar. Our calculations agree with reported trend for the experimentally determined enthalpies of formation of $(BA)_2(MA)_{n-1}Pb_nI_{3n+1}$ which show that the formation enthalpies for structures with an even number of layers are significantly more exothermic than those for odd values of n, i.e. the formation enthalpy of n=2 is more negative than that of n=1 and n=3.[38]

Additionally, it is important to highlight that lower n (n=1, 2) RPP typically exhibit strain due to the lack of rotational degrees of freedom of surface octahedra which prevents strain relaxation.[33] Our DFT calculations, see **Figure 1b** and Table S3, show that $(BA_{0.5}PEA_{0.5})_2MAPb2Br_7$ exhibits the smallest strain, compared to pure BA and pure PEA spacer cations, which is expected to result in reduced formation of defects and enhanced light emission. Finally, as shown in **Figure 1c**, smaller e-ph coupling was found for n=2 BA-PEA mixed RPP, compared to pure BA and PEA, which might contribute to the emission enhancement and/or improved stability of photoluminescence and electroluminescence. As shown in Figure S1, e-ph coupling is due to low frequency vibrations of inorganic frame[32] (<200 cm^{-1}) and coupled vibrations of organic cations.

Figure 2 shows the absorption and PL spectra and XRD patterns of $BA_2MA_{n-1}Pb_nBr_{3n+1}$, $PEA_2MA_{n-1}Pb_nBr_{3n+1}$ and $(BA_{0.5}PEA_{0.5})_2MAPb_2Br_7$ thin films prepared from solutions corresponding to n=2 stoichiometry. In the case of BA-perovskite, high phase purity of n=2 phase is evident from the absorption spectra as well as a prominent blue emission in the PL spectra (**Figure 2a**). Asymmetric line shape does not necessarily indicate the presence of additional phases since it is commonly observed in n=1 RPPs which only have one phase, and it occurs due to strong exciton-phonon coupling.[27] The formation of pure phase BA films is also supported by the estimation of formation enthalpy as shown in **Figure 1a**. The

enthalpies are calculated from the molecular dynamics simulations and therefore, in contrast to common static T=0 K approaches, room temperature contributions are also included. It can be observed that both temperature contributions as well as contributions of van der Waals forces are very significant (**Figure 1a, Table S1)** thus quite a different stability landscape would have been obtained if those contributions are marginalised. Additionally, XRD also confirmed that the only phase present is $BA_2MAPb_2Br_7$ (n=2) (**Figure 2d**). The structure has been refined in *Ama*2 space group exhibiting the periodicity 38.72(3) Å along the *c*-direction. The value of *c* parameter is slightly smaller, as expected due to the smaller radii of Br^-, compared to its iodine analogue $BA_2MAPb_2I_7$ reported by Stoumpos *et al*.[5]

For PEA-based RPP films prepared with solution stoichiometry corresponding to n=2, we observe a significant presence of the n=1 phase in the absorption spectra together with the excitonic features corresponding to n=2 and n=3 (**Figure 2b**). The presence of multiple n phases is common for $PEA_2MA_{n-1}Pb_nX_{3n+1}$.[17, 20, 23,30] The prominent presence of n=1 phase is additionally confirmed by XRD. For the full pattern decomposition shown in **Figure 2e**, the unit-cell parameters of iodide analogue[39,40] has been used as a starting structural model. The refinement showed that that *c*-parameter of PEA_2PbBr_4 amounts to 17.53(1) Å which is slightly smaller than 17.69 Å reported in the case of PEA_2PbI_4.[39] Although n=1 is dominant phase, the observed luminescence from PEA-based samples is green, which is attributed to energy funneling, i.e. the energy transfers to a small amount of the highest n phase. The fact that PEA sample showed the presence of n=1-3 phases, while the BA exclusively contains only n=2, is attributed to the negligible differences in the formation enthalpies for n=1, 2 and 3 phases at RT in the case of PEA (**Figure 1a**). Additionally, both the T-shaped[13] and π-π stacking arrangements[41] of PEA molecules within the spacer bilayer have been considered; computational structural relaxation favours T-shaped arrangement as minimum energy structure for n=1, while for higher n minimum energy structure contains π-π ordered PEA molecules (**Table S2**, Supporting Information). As a consequence, e-ph coupling for n=2 and

n=3 is 1-order of magnitude larger than the coupling for *n*=1. This indicates that previously reported tremendous difference in PLQY for PEA perovskites compared to BA (17% for BA-based and 79% for PEA-based 2D perovskite)[1,13] would only hold for *n*=1 (excluding any contributions of energy funneling effect to the emission in films with multiple *n* phases).

From the absorption spectra of $(BA_{0.5}PEA_{0.5})_2MAPb_2Br_7$ shown in **Figure 2c** we can observe that, similar to BA- and opposite from PEA-based samples, we obtain high phase purity material corresponding exclusively to *n*=2. This is different from a previous report, where the addition of up to 60% of iso-propylammonium bromide failed to result in the formation of phase-pure PEA-based RPP.[23] Structural features of prepared mixed BA-PEA *n*=2 perovskite thin film have additionally been investigated by XRD as shown in **Figure 2d** and **Figure S2**. **Figure S2** shows XRD pattern of $(BA_{0.5}PEA_{0.5})_2MAPb_2Br_7$ compared to the $BA_2MAPb_2Br_7$ pattern and to the pattern calculated from published structure $PEA_2MAPb_2I_7$.[39] Ideally, one should make this comparison by using the pattern $PEA_2MAPb_2Br_7$ instead of $PEA_2MAPb_2I_7$, however in the scope of our work *n*=2 PEA bromide-based perovskite has not been obtained (we obtained *n*=1 as a dominant phase), nor is bromide-based structure known from the literature. Nevertheless, it is reasonable to assume that PEA-based bromide perovskite would show only small shifts in line positions compared to iodide analogue. From **Figure S2** it is obvious that mixed compound has indeed formed, since the XRD pattern of mixed perovskite is different compared to those of its end members (BA- and PEA-based perovskite). Additionally, significant line broadening can be noticed in XRD pattern of mixed- compared to single cation- perovskites that likely arose from the competition of the two ammonium cations to occupy the allocated positions in the perovskite lattice. Full pattern decomposition (**Figure 1f**) has been performed by using the structural model as obtained by the DFT. DFT optimization of cell parameters as well as all atomic coordinates have been performed on the starting model that is built by considering the unit cell of PEA perovskite in which every second PEA molecule is substituted by BA molecule. Combined DFT and XRD study

revealed that new mixed BA-PEA material crystallizes in a triclinic system, space group P1 with lattice parameters a=8.411(3) Å, b=8.176(2) Å, c=21.991(5) Å, α=97.37(1)°, β=100.04(2)° and γ=89.28(1)°. Determined c-parameter of $(BA_{0.5}PEA_{0.5})_2MAPb_2Br_7$ is similar to the c-parameter of parent PEA structure (22.76 Å for iodine analogue).[39] This is expected if one considers that the assembly of mixed spacer bilayer has to be dominated by the longer ammonium cation. The presence of both PEA and BA cations has also been confirmed by NMR measurements, as shown in **Figure 1g**. The molar ratio of PEA:BA:MA was calculated to be 1:1:1 which agrees with the stoichiometry of $(BA_{0.5}PEA_{0.5})_2MAPb_2Br_7$. We also investigated the composition of the films prepared with different ratio of PEA and BA. For lower PEA content (i.e. 0.25, 0.50), only n=2 excitonic feature in the absorption spectra, as shown in **Figure S3**, Supporting Information. With increased PEA content (0.75), we can observe the appearance of n=1 phase. Those findings indicate that the ratio of two cations might play a determining role in the stabilization of n=2 mixed perovskite material. While the incorporation of PEA cations leads to enhanced PL and improved thermal stability of BA-PEA perovskite compared to pure BA perovskite, once PEA content becomes too large, the stabilizing effect diminishes thus resulting in the crystallization of multiple n mixture. This behaviour is likely to be caused by the fact that PEA cation, unlike BA, is often disordered. [39] The concept of having perovskite material containing two different cations in spacer bilayer can also be demonstrated for n=1 as shown in **Figure S4**, Supporting Information. In agreement with calculated formation enthalpies of BA_2PbBr_4 and PEA_2PbBr_4, that are lower than the formation energy of $(BA_{0.5}PEA_{0.5})_2PbBr_4$, we obtained a mixture of all three phases. Deposition method altering crystallization kinetics and favouring more rapid nucleation, such as vacuum drying, blow-drying and the use of anti solvent reduce the proportion of BA_2PbBr_4 and PEA_2PbBr_4 phases, as shown in **Figure S5**, Supporting Information. Thus, we clearly show that mixed spacer cations lead to the formation of distinctly different crystal structure.

Our theoretical calculations also predict superior optical properties due to lower strain and lower e-ph coupling in mixed cation samples. Experimentally, we indeed obtained higher luminescence from the $(BA_{0.5}PEA_{0.5})_2MAPb_2Br_7$ compared to $BA_2MAPb_2Br_7$ films, while the films have comparable thickness (174±12 nm and 185±16 nm, respectively). However, luminescence intensity is also dependent on the native defects in the films, which are affected by the deposition conditions. Therefore, we performed comprehensive optimization of the film deposition conditions for $(BA_{0.5}PEA_{0.5})_2MAPb_2Br_7$ and $BA_2MAPb_2Br_7$ films, including investigating the factors known to affect crystallization and/or optical quality, such as the effects of precursor purity, solvents and/or additives used, and the use of anti solvents.[18,29,30,42-46] The details are given in Supporting Information, **Note 1** and **Figures S6-S12**.

Figure 3 clearly illustrates advantages of the utilization of *n*=2 mixed perovskite for blue-emitting applications over pure *n*=2 BA material. From the PL spectra of optimized films shown in **Figure 3a** we can observe that mixed spacer cation films exhibit higher PL intensity compared to BA sample. The enhancement of emission is also confirmed by obtained values of photoluminescence quantum yield (PLQY), 2.80±0.28% for $(BA_{0.5}PEA_{0.5})_2MAPb_2Br_7$ thin films and 1.66±0.52% for $BA_2MAPb_2Br_7$ thin films (averages of 5 samples each). To further characterize the samples, we performed time-resolved photoluminescence (TRPL) measurements, as shown in **Figure S13** and summarized in **Table S4**. The PL decay curves can be described with a commonly used bi-exponential decay, and the two samples exhibit similar average lifetimes τ_{avg}. From the measured PLQY and determined τ_{avg} we can estimate radiative recombination rate k_{rad} as k_{rad}=PLQY/τ_{avg}.[47] The obtained results of 2.55 ⊣10^6 s^{-1} and 5.0 ⊣10^6 s^{-1} indicate higher radiative recombination in $(BA_{0.5}PEA_{0.5})_2MAPb_2Br_7$ thin films, despite lower grain sizes compared to $BA_2MAPb_2Br_7$ thin films, as shown in SEM images of films on ITO substrates in **Figure S14a** and **S14b**, Supporting Information.

We also investigated environmental (**Figure 3b**, **3c** and **3f**) and thermal stability (**Figure 3d** and **3e**) since those aspects have significant impact on the device applications. It is

known that the emission of lead halide perovskites can shift under UV or laser irradiation in ambient, as documented in mixed halide 3D perovskites,[23] perovskite nanoplatelets,[46] and Ruddlesden-Popper perovskites.[12] Mixed perovskite films do not show any shifts of emission peak under 325 nm laser illumination when encapsulated, as shown in **Figure 3f,** similar as in the case of BA-compound shown in **Figure S15**, Supporting information. In ambient conditions, we observe red shift of the emission peak and the reduction of the emission intensity over time as shown in **Figure 3b** and **3c** for both BA- and mixed perovskite. That is consistent with previously reported phenomena of photobleaching and transformation in *n*=2 MAPbBr nanoplatelets.[41] The same behavior is also observed in $BA_2MAPb_2Br_7$ single crystals, as shown in **Figure S15**, Supporting Information. The transformation phenomenon, i.e. the appearance of features corresponding to different *n* values, has been attributed to humidity.[41] Humidity also induces the change of the phase composition over time without UV illumination.[18,24] Nevertheless, the observed red shift in mixed cation films is smaller and slower when exposed to UV laser in ambient clearly illustrating the improved environmental stability compared to pure BA films. In addition to improved ambient stability, mixed cation films also exhibit enhanced thermal stability, which is important for LED applications due to Joule heating during operation.[28] While annealed $BA_2MAPb_2Br_7$ films show additional peaks in both PL (**Figure 3d**) and absorption spectra (**Figure S16**, Supporting information) corresponding to *n*=3 (PL) and *n*=1 (absorption) phases, annealed $(BA_{0.5}PEA_{0.5})_2MAPb_2Br_7$ films remain stable at elevated temperatures as evidenced from **Figure 3e**. Enhanced thermal stability is also critical for successful fabrication of blue-emitting LEDs since the temperature rises up to ~70ºC during the deposition of Cs_2CO_3 and even up to ~95ºC during the deposition of LiF layers of the electrode. This leads to emission peak shifts, as illustrated in **Figure S17**, Supporting Information. Such pronounced red shifts of EL spectra compared to PL spectra, as observed for BA film, are typically observed in films with inferior ambient and thermal stability, while mixed spacer cation films can retain blue emission.

Due to their promising optical properties, we have investigated the application of optimized $(BA_{0.5}PEA_{0.5})_2MAPb_2Br_7$ films to obtain deep-blue LEDs. Device architecture is shown in **Figure S18, Supporting Information**, while SEM of the $(BA_{0.5}PEA_{0.5})_2MAPb_2Br_7$ and $BA_2MAPb_2Br_7$ on the hole transport layer (HTL) and I-V curves of hole-only devices are shown in **Figure S14c, S14d** and **S19**, Supporting Information. Both BA-PEA and pure BA samples exhibit comparable efficiency of the order of 10^{-2}% (**Figure 4a** and **4b**) and in both cases the EQE exhibited a roll-off, which is common in perovskite LEDs,[21,23,26,28] and it can be attributed to non-radiative defects[28] and Auger recombination.[26] The efficiency could likely be further improved with optimization of the film morphology on the HTL, since the films on ITO exhibit lower surface roughness and fewer defects (aggregates, pinholes). It can be seen that $BA_2MAPb_2Br_7$ devices exhibit a maximum EQE of 0.026% (average value of 0.013±0.009% for five devices). However, due to inherent instability of BA-based films when exposed to elevated temperature during electrode deposition in LED fabrication, the EL emission peak has shifted to 468 nm, with corresponding CIE coordinates of (0.132, 0.104). In contrast, the peak position of mixed BA-PEA device is centered at 456 nm with CIE coordinates of (0.156, 0.088) which is very close to the NTSC blue standard of (0.14, 0.08). The mixed cation devices exhibit a very small shift between PL and EL spectra, as shown in Fig. 4c, but the pure blue emission is obtained in both cases. Furthermore, there is an obvious peak shift between PL and EL spectra of BA-based devices (Figure 4d), and the emission shifts from pure blue PL to sky-blue EL. The maximum EQE of $(BA_{0.5}PEA_{0.5})_2MAPb_2Br_7$ is to 0.015% (average value of 0.012%±0.001 which is two times higher than previously reported blue emission LED from the BA-based RPP exhibiting multiple peaks with dominant emission at ~450 nm, poor spectral stability and the efficiency of 0.0054%[21] indicating significant progress towards the achievement of pure blue emission in a quasi-2D RPP emitter without halogen mixing. Moreover, despite the fact that high spectral stability in blue-emitting perovskite LEDs has been scarce,[23,28] both of our devices exhibit excellent spectral

stability over time as well as bias voltage, as shown in **Figure 4e, 4f** for $(BA_{0.5}PEA_{0.5})_2MAPb_2Br_7$ and **Figure S19 b and c**, Supporting Information for $BA_2MAPb_2Br_7$. Furthermore, both BA and BA-PEA based devices exhibit exponential decay of emission intensity, as shown in **Figure S20**, Supporting Information. The obtained time constants τ and the corresponding T_{50} are τ =47.3 s and T_{50}=70.6 for BA-based device, and τ =100.7 s and T_{50}=91.4 for BA-PEA based device, illustrating the improved stability of mixed cation film. The obtained value of T_{50} of ~1.5 min is comparable to that typically reported for blue perovskite LEDs (several minutes, longer T_{50} for longer wavelength).[23,28] Finally, it should also be noted that the mixed cation approach is not only applicable to BA-PEA cation combination, but also to other cations. The generalization of mixed spacer cation approach for stabilization of *n*=2 phase is demonstrated for different spacer cation combinations (benzylammonium (BZA) and BA, 4-fluoro-phenethylammonium (FPEA) and BA), as shown in **Figure S21**, Supporting Information.

Thus, we demonstrate the use of two different spacer cations to obtain an RPP with a mixed bilayer which exhibits distinct advantages over RPP materials with a single spacer cation, in terms of phase purity, light emission intensity, as well as ambient and thermal stability. Based on comprehensive DFT calculations including *ab-initio* molecular dynamics, we attribute improved properties to more favorable formation enthalpy of *n*=2 phase, lower strain and lower e-ph coupling. The approach is applicable to other combinations of spacer cations, although the optimization of deposition conditions can be needed to enhance phase purity.

Supporting Information
Supporting Information is available from the Wiley Online Library or from the author.

Acknowledgements
This work was supported by the Seed Funding for Basic Research and Seed Funding for Strategic Interdisciplinary Research Scheme of the University of Hong Kong. The authors also acknowledge financial support from Shenzhen Science and Technology Commission

Projects No. JCYJ20160530184523244 and JCYJ20170818141216288, European Union through the European Regional Development Fund - the Competitiveness and Cohesion Operational Programme (KK.01.1.1.06), and Croatian–Chinese bilateral projects entitled "Insight into thermosalient phenomenon of molecular crystals – one step closer to revealing the jumping mystery using the high-temperature AFM and high-temperature FTIR" and "The study of highly stable and mixed cations organometallic trihalide perovskite materials and solar cells". The authors would like to thank Dr. K. H. Low (Chemistry, HKU) for performing XRD measurements, Dr. Maggie Chan and Prof. V. W.W. Yam (Chemistry, HKU) for access to facilities and LED characterization measurements.

Received: ((will be filled in by the editorial staff))
Revised: ((will be filled in by the editorial staff))
Published online: ((will be filled in by the editorial staff))

References

[1] Z. Chen, Y. Guo, E. Wertz, J. Shi, *Adv. Mater.* **2018**, *30*, 1803514.

[2] J. Hu, L. Yan, W. You, *Adv. Mater.* **2018**, *30*, 1802041.

[3] L. N. Quan, F. P. Garcia de Arquer, R. P. Sabatini, E. H. Sargent, *Adv. Mater.* **2018**, *30*, 1801996.

[4] N. K. Kumawat, X. K. Liu, D. Kabra, F. Gao, *Nanoscale* **2019**, *11*, 2109.

[5] C. C. Stoumpos, D. H. Cao, D. J. Clark, J. Young, J. M. Rondinelli, J. I. Jang, J. T. Hupp, M. G. Kanatzidis, *Chem. Mater.* **2016**, *28*, 2852.

[6] X. Zhang, R. Munir, Z. Xu, Y. C. Liu, H. H. Tsai, W. Y. Nie, J. B. Li, T. Q. Niu, D. M. Smilgies, M. G. Kanatzidis, A. D. Mohite, K. Zhao, A. Amassian, S. Z. (F.) Liu, *Adv. Mater.* **2018**, *30*, 1707166.

[7] D. H. Cao, C. C. Stoumpos, O. K. Farha, J. T. Hupp, M. G. Kanatzidis, *J. Am. Chem. Soc.* **2015** *137*, 7843.

[8] X. Q. Zhang, G. Wu, S. D. Yang, W. F. Fu, Z. Q. Zhang, C. Chen, W. Q. Liu, J. L. Yan, W. T. Yang, H. Z. Chen, *Small* **2017**, *13*, 1700611.

[9] N. R. Venkatesan, J. G. Labram, M. L. Chabinyc, *ACS Energy Lett.* **2018**, *3*, 380.

[10 L. Yan, J. Hu, Z. Guo, H. Chen, M. F. Toney, A. M. Moran, W. You, *ACS Appl. Mater. Interfaces* **2018**, *10*, 33187.

[11] P. Vashishtha, M. Ng, S. B. Shivarudraiah, J. E. Halpert, *Chem. Mater.* **2019**, *31*, 83.

[12] K. Leng, I. Abdelwahab, I. Verzhbitskiy, M. Telychko, L. Chu, W. Fu, X. Chi, N. Guo, Z. Chen, Z. Chen, C. Zhang, G. H. Xu, J. Lu, M. Chhowalla, G. Eda, K. P. Loh, *Nature Mater.* **2018**, *17*, 908.

[13] X. Gong, O. Voznyy, A. Jain, W. Liu, R. Sabatini, Z. Piontkowsky, G. Walters, G. Bappi, S. Nokhrin, O. Bushuyev, M. Yuan, R. Comin, D. McCamant, S. O. Kelley, E. H. Sargent, *Nature Mater.* **2018**, *17*, 550.

[14] X. Zhang, G. Wu, W. Fu, M. Qin, W. Yang, J. Yan, Z. Zhang, X. Lu, H. Chen, *Adv. Energy Mater.* **2018**, *8*, 1702498.

[15] W. Peng, J. Yin, K. T. Ho, O. Ouellette, M. D. Bastiani, B. Murali, O. E. Tall, C. Shen, X. H. Miao, J. Pan, E. Alarousu, J. H. He, B. S. Ooi, O. F. Mohammed, E. Sargent, O. M. Bakr, *Nano Lett.* **2017**, *17*, 4759.

[16] J. Byun, H. Cho, C. Wolf, M. Jang, A. Sadhanala, R. H. Friend, H. Yang, T. W. Lee, *Adv. Mater.* **2016**, *28*, 7515.

[17] M. Yuan, L. N. Quan, R. Comin, G. Walters, R. Sabatini, O. Voznyy, S. Hoogland, Y. Zhao, E. M. Beauregard, P. Kanjanaboos, Z. Lu, D. H. Kim, E. H. Sargent, *Nat. Nanotechnol.* **2016**, *11*, 872.

[18] Y. T. Zou, Q. Huang, Y. G. Yang, M. Y. Ban, S. Y. Li, Y. J. Han, T. Wu, Y. S. Tan, X. Y. Gao, T. Song, B. Q. Sun, *Adv. Mater. Interfaces* **2018**, *5*, 1801030.

[19] W. Fu, J. Wang, L. Zuo, K. Gao, F. Liu, D. S. Ginger, A. K. Y. Jen, *ACS Energy Lett.* **2018**, *3*, 2086.

[20] L. N. Quan, Y. Zhao, F. P. G. deArquer, R. Sabatini, G. Walters, O. Voznyy, R. Comin, Y. Li, J. Z. Fan, H. Tan, J. Pan, *Nano Lett.* **2017**, *17*, 3701.

[21] D. N. Congreve, M. C. Weidman, M. Seitz, W. Paritmongkol, N. S. Dahod, W. A. Tisdale, *ACS Photonics* **2017**, *4*, 476.

[22] P. Cai, X. Wang, H. J. Seo, X. Yan, *Appl. Phys. Lett.* **2018**, *112*, 15.

[23] J. Xing, Y. Zhao, M. Askerka, L. N. Quan, X. Gong, W. Zhao, J. Zhao, H. Tan, G. Long, L. Gao, Z. Yang, O. Voznyy, J. Tang, Z. H. Lu, Q. Xiong, E. H. Sargent, *Nat. Commun.* **2018**, *9*, 3541.

[24] C. Stoumpos, C. M. M. Soe, H. Tsai, W. Nie, J. C. Blancon, D. H. Cao, F. Liu, B. Traoré, C. Katan, J. Even, A. D. Mohite, M. G. Kanatzidis, *Chem* **2017**, *2*, 427.

[25] Q. Wang, J. Ren, X. F. Peng, X. X. Ji, X. H. Yang, *ACS Appl. Mater. Interfaces* **2017**, *9*, 29901.

[26] Z. M. Chen, C. Y. Zhang, X. F. Jiang, M. Y. Liu, R. X. Xia, T. T. Shi, D. C. Chen, Q. F. Xue, Y. J. Zhao, S. J. Su, H. L. Yip, Y. Cao, *Adv. Mater.* **2017**, *29*, 1603157.

[27] L. M. Ni, U. Huynh, A. Cheminal, T. H. Thomas, R. Shivanna, T. F. Hinrichsen, S. Ahmad, A. Sadhanala, A. Rao, *ACS Nano* **2017**, *11*, 10834.

[28] Y. Z. Jiang, C. C. Qin, M. H. Cui, T. W. He, K. K. Liu, Y. M. Huang, M. H. Luo, L. Zhang, H. Y. Xu, S. S. Li, J. L. Wei, Z. Y. Liu, H. H. Wang, G. H. Kim, M. J. Yuan, J. Chen, *Nat. Commun.* **2019**, *10*, 1868.

[29] C. J. Dahlman, R. A. DeCrescent, N. R. Venkatesan, R. M. Kennard, G. Wu, M. A. Everest, J. A. Schuler, M. L. Chabinyc, *Chem. Mater.* **2019**, *31*, 5832.

[30] R. Quintero-Bermudez, A. Gold-Parker, A. H. Proppe, R. Munir, Z. Yang, S. O. Kelly, A. Amassian, M. F. Toney, E. H. Sargent, *Nature Mater.* **2018**, *17*, 900.

[31] T. Y. Li, A. M. Zeidell, G. Findik, W. A. Dunlap-Shohl, J. Euvrard, K. Gundogdu, O. D. Jurchescu, D. B. Mitzi, *Chem. Mater.* **2019**, *31*,4267.

[32]F. Thouin, D. A. Valverde-Chàvez, C. Quarti, D. Cortecchia, I. Bargigia, D. Beljonne, A. Petrozza, C. Silva, A. R. S. Kandada, *Nature Mater.* **2018**, *18*, 349.

[33] M. Kepenekian, B. Traore, J. C. Blancon, L. Pedesseau, H. Tsai, W. Nie, C. C. Stoumpos, M. G. Kanatzidis, J. Even, A. D. Mohite, S. Tretiak, *Nano Lett.* **2018**, *18*, 5603.

[34] K. Miyata, D. Meggiolaro, M. T. Trinh, P. P. Joshi, E. Mosconi, S. C. Jones, F. De Angelis, X. Y. Zhu, "Large polarons in lead halide perovskites", *Sci. Adv.* **2017**, *3*, e1701217.

[35] S. Chen, N. Shen, L. Z. Zhang, W. G. Kong, L. Zhang, C. Cheng, B. Xu, *J. Mater. Chem. A* **2019**, *7*, 9542.

[36] M. Z. Long, T. K. Zhang, D. C. Chen, M. C. Qin, Z. F. Chen, L. Gong, X. H. Lu, F. Y. Xie, W. Xie, J. Chen, J. B. Xu, *ACS Energy Lett* **2019**, *4*, 1025.

[37] J. Qiu, Y. D. Xia, Y. T. Zheng, W. Hui, H. Gu, W. B. Yuan, H. Yu, L. F. Chao, T. T. Nou, Y. G. Yang, X. Y. Gao, Y. H. Chen, W. Huang, *ACS Energy Lett*, **2019**, *4*, 1513.

[38] C. M. M. Soe, G. P. Nagabhushana, R. Shivaramaiah, H. Tsai, W. Nie, J.-C. Blancon, F. Melkonyan, H. H. Cao, B. Traoré, L. Pedesseau, M. Kepenekian, C. Katan, J. Even, T. J. Marks, A. Navrotsky, A. D. Mohite, C. C. Stoumpos, M. G. Kanatzidis, *Proc. Natl. Acad. Sci. U. S. A.* **2019**, *116*, 58.

[39] J. Calabrese, N. L. Jones, R. L. Harlow, N. Herron, D. L. Thorn, Y. Wang, *J. Am. Chem. Soc.* **1991**, *113*, 2328.

[40] I. C. Smith, E. T. Hoke, D. Solis-Ibarra, M. D. McGehee, H. I. Karunadasa, *Angew. Chem., Int. Ed.* **2014**, *53*, 11232.

[41] A. H. Slavney, R. W. Smaha, I. C. Smith, A. Jaffe, D. Umeyama, H. I. Karundasa, *Inorg. Chem.* **2017**, *56*, 46.

[42] J. T. Tisdale, T. Smith, J. R. Salasin, M. Ahmadi, N. Johnson, A. V. Ievlev, M. Koehler, C. J. Rawn, E. Lukosi, B. Hu, *CrystEngComm* **2018**, *20*, 7818.

[43] Y. H. Hu, L. M. Spies, D. Alonso-Alvarez, P. Mocherla, H. Jones, J. Hanisch, T. Bein, P. R. F. Barnes, P. Docampo, *J. Mater. Chem. A* **2018**, *6*, 22215.

[44] F. Yang, G. Kapil, P. Zhang, Z. S. Hu, M. A. Kamarudin, T. L. Ma, S. Hayase, *ACS Appl. Mater. Interfaces* **2018**, *10*, 16482.

[45] S. Masi, F. Aiello, A. Listorti, F. Balzano, D. Altamura, C. Giannini, R. Caliandro, G. Uccello-Barretta, A. Rizzo, S. Colella, *Chem. Sci.* **2018**, *9*, 3200.

[46] S. K. Hu, C. M. Mauck, W. A. Tisdale, *Chem. Mater.* **2019**, *31*, 2486.

[47] Z. G. Xiao, R. A. Kerner, N. Tran, L. F. Zhao, G. D. Scholes, B. P. Rand, *Adv. Funct. Mater.* **2019**, *29*, 1807284.

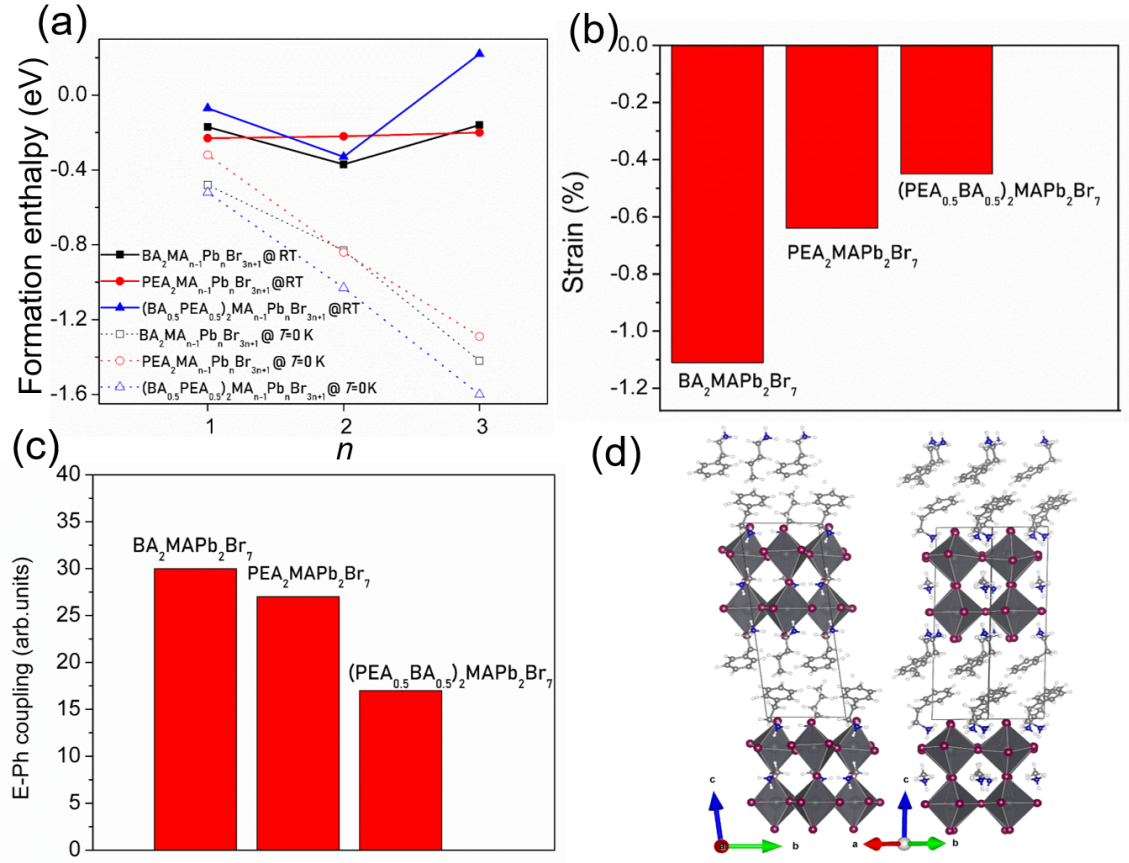

Figure 1. a) Formation enthalpies for $BA_2MA_{n-1}Pb_nBr_{3n-1}$, $PEA_2MA_{n-1}Pb_nBr_{3n-1}$ and $(BA_{0.5}PEA_{0.5})_2MA_{n-1}Pb_nBr_{3n-1}$. Full symbols represent enthalpies calculated at RT while the hollow symbols show enthalpies calculated at 0 K. b) Strain for $BA_2MAPb_2Br_7$, $PEA_2MAPb_2Br_7$ and $(BA_{0.5}PEA_{0.5})_2MAPb_2Br_7$ c) E-Ph coupling for $BA_2MAPb_2Br_7$, $PEA_2MAPb_2Br_7$ and $(BA_{0.5}PEA_{0.5})_2MAPb_2Br_7$, d) structure of $(BA_{0.5}PEA_{0.5})_2MAPb_2Br_7$

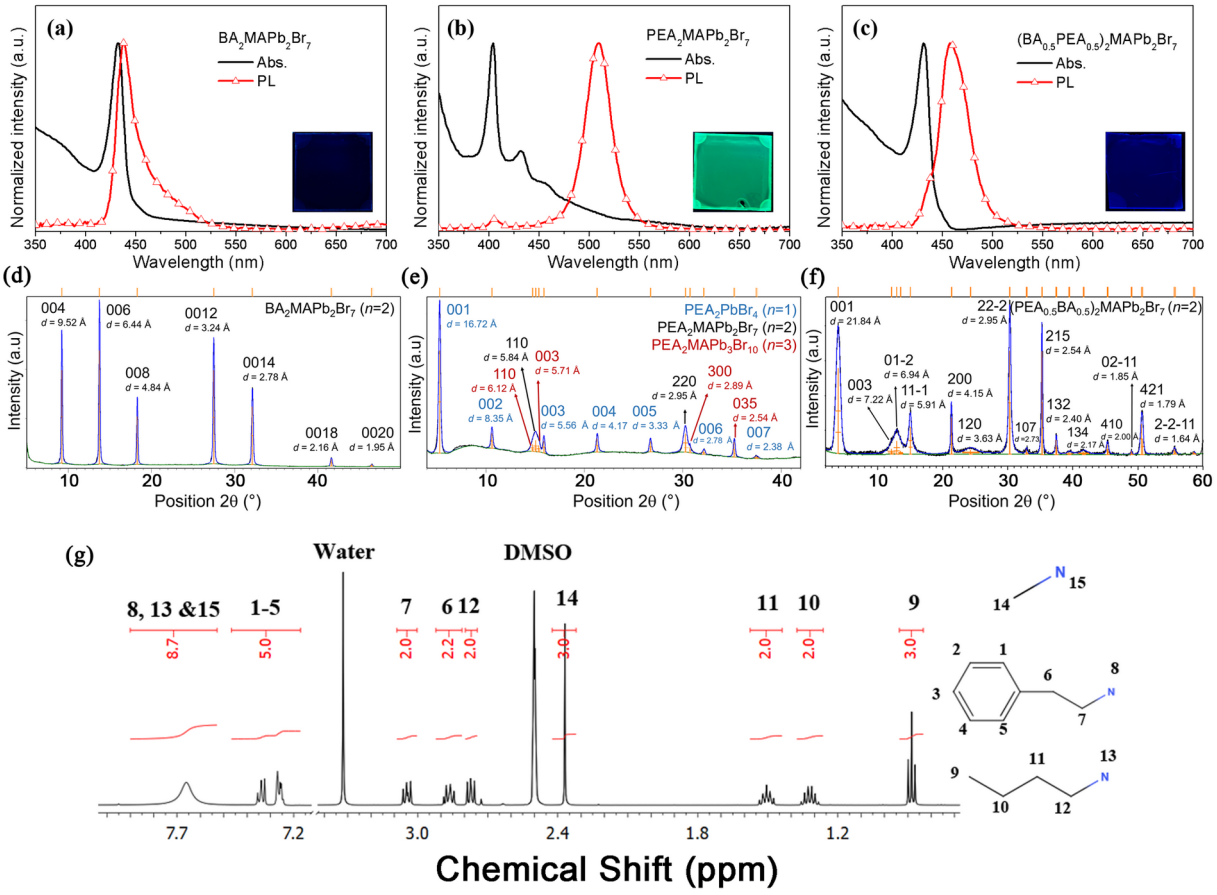

Figure 2. Absorption and PL spectra a) $BA_2MAPb_2Br_7$, b) $PEA_2MA_{n-1}Pb_nBr_{3n+1}$ and c) $(BA_{0.5}PEA_{0.5})_2MAPb_2Br_7$ films prepared with precursor solution of n=2 stoichiometr;. XRD patterns of d) $BA_2MAPb_2Br_7$, e) $PEA_2MA_{n-1}Pb_nBr_{3n+1}$, and f) $(BA_{0.5}PEA_{0.5})_2MAPb_2Br_7$ films prepared with precursor solution of n=2 stoichiometry; g) H-NMR spectrum of $(BA_{0.5}PEA_{0.5})_2MAPb_2Br_7$ mixed perovskite film dissolved in DMSO-d6. The peaks were assigned with corresponding atoms.

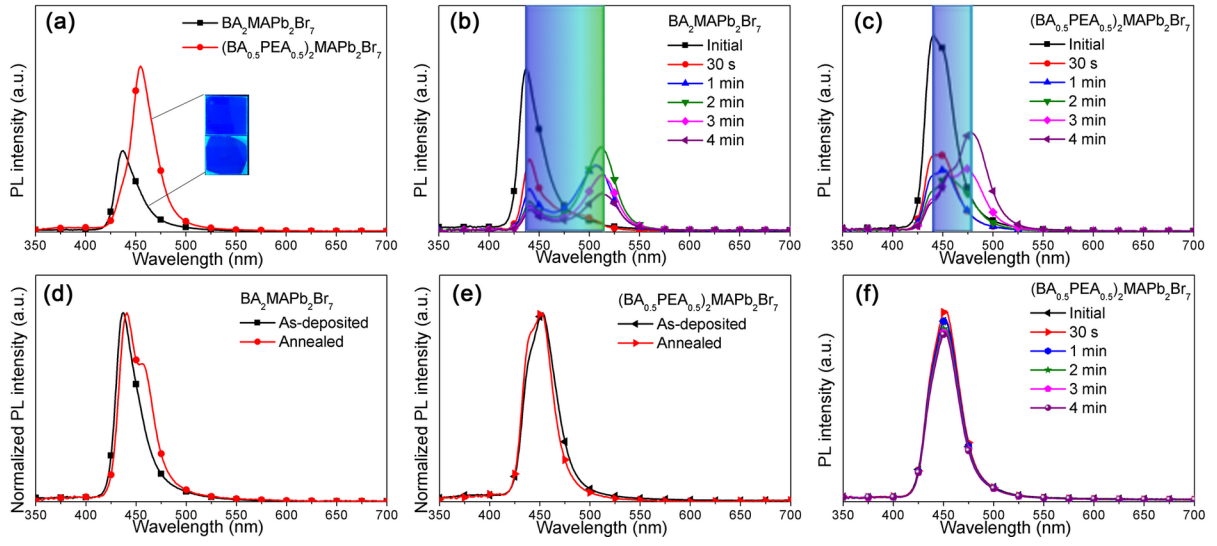

Figure 3. a) PL spectra of $BA_2MAPb_2Br_7$ and $(BA_{0.5}PEA_{0.5})_2MAPb_2Br_7$ thin films with optimized deposition conditions; the inset shows corresponding photos. PL spectra after different durations of laser exposure in ambient for b) $BA_2MAPb_2Br_7$ and c) $(BA_{0.5}PEA_{0.5})_2MAPb_2Br_7$ films; Corresponding peak colours are indicated. PL spectra of as-deposited and annealed d) $BA_2MAPb_2Br_7$ and e) $(BA_{0.5}PEA_{0.5})_2MAPb_2Br_7$ films; f) PL spectra of encapsulated $(BA_{0.5}PEA_{0.5})_2MAPb_2Br_7$ films after different durations of laser exposure.

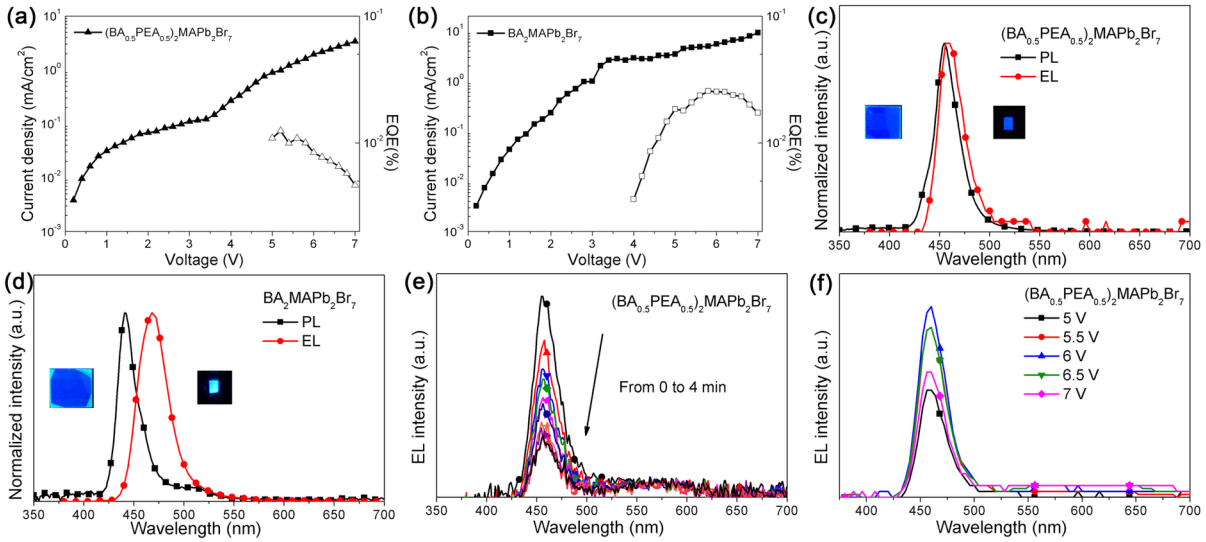

Figure 4. a, b) I-V and EQE versus voltage bias for $BA_2MAPb_2Br_7$ and $(BA_{0.5}PEA_{0.5})_2MAPb_2Br_7$ devices, respectively; c, d)) EL and PL spectra of $BA_2MAPb_2Br_7$ and $(BA_{0.5}PEA_{0.5})_2MAPb_2Br_7$ devices, respectively. The insets show corresponding photos. e) EL spectra of $(BA_{0.5}PEA_{0.5})_2MAPb_2Br_7$ device after different time intervals. f) EL spectra of $(BA_{0.5}PEA_{0.5})_2MAPb_2Br_7$ device under different voltage bias.

Ruddlesden-Popper halide perovskite (RPP) materials are promising candidates for light emitting devices with tunable emission wavelength. However, pure blue emission n=2 RPP films are unstable for LED applications. The stabilization of n=2 phase is demonstrated by employing two spacer cations to form a mixed cation bilayer structure. Pure blue LEDs are achieved with excellent spectral stability.

Keyword
Ruddlesden-Popper, quasi-2D perovskites, perovskite light-emitting diodes, blue emission

Tik Lun Leung, Ho Won Tam, Fangzhou Liu, Jingyang Lin, Alan Man Ching Ng, Wai Kin Chan, Wei Chen, Zhubing He, Ivor Lončarić, Luca Grisanti, Chao Ma, Kam Sing Wong, Ying Suet Lau, Furong Zhu, Željko Skoko, Jasminka Popović,* and Aleksandra B. Djurišić*

Mixed spacer cation stabilization of blue-emitting n=2 Ruddlesden-Popper organic-inorganic halide perovskite films

ToC figure